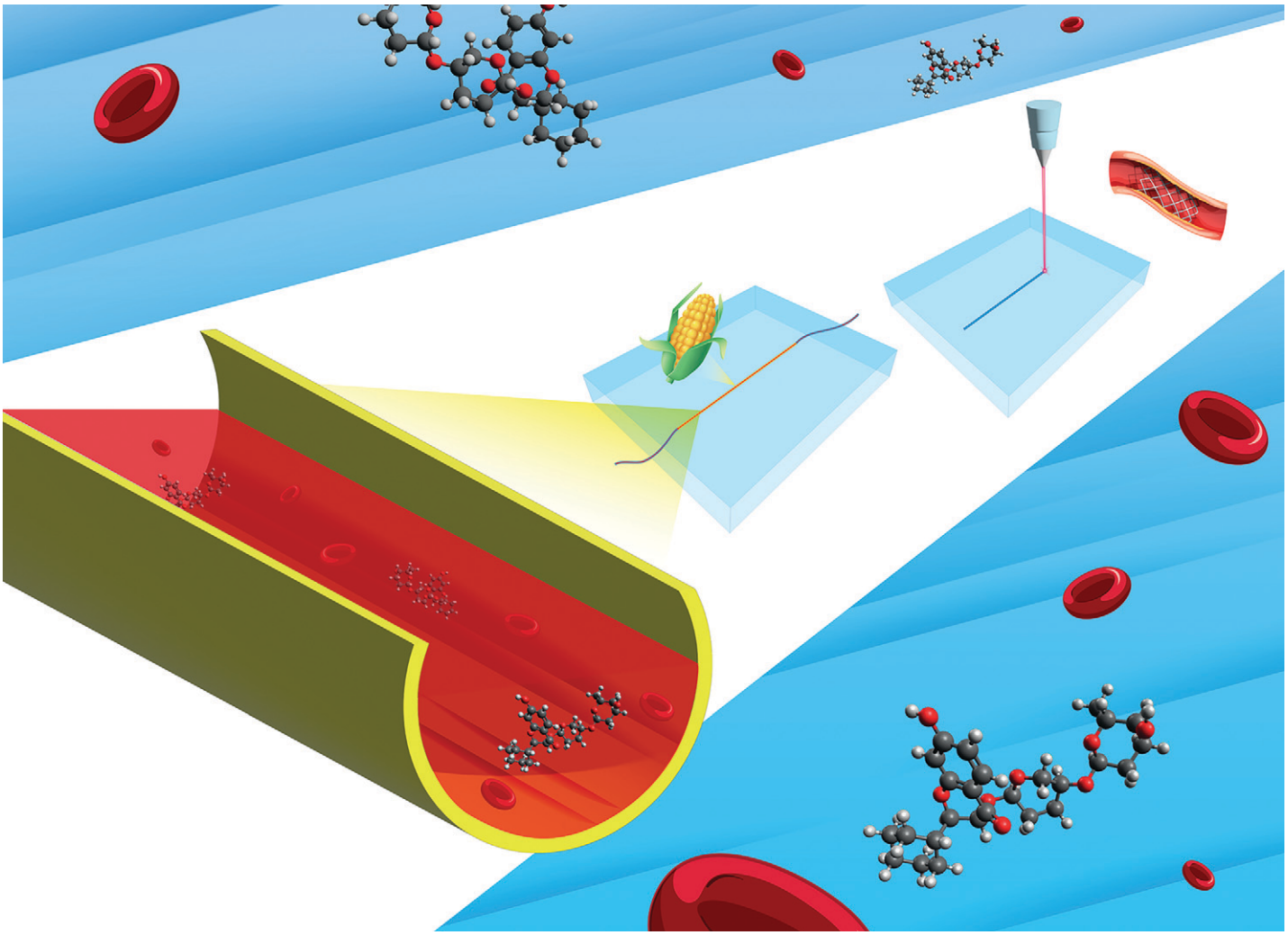

Featuring work from Dr. Athanassiou's laboratory, Smart Materials Group, Italian Institute of Technology, Genoa, Italy.

Dynamic investigation of zein-based degradable and hemocompatible coatings for drug-eluting stents: a microfluidic approach

Drug-loaded zein-based coatings were deposited onto fused silica-based channels designed to mimic the microenvironment of a stented vessel and fabricated by femtosecond-laser-assisted micromachining. The investigation of the dynamic behaviour of the coatings in terms of drug release and matrix degradation was carried out in the presence of simulated blood fluids. Moreover, in-flow whole blood tests performed with the proposed reusable platforms showed a significant reduction of blood cells and platelet adhesion, confirming the benefits of using such naturally-derived coatings for hemocompatible drug-eluting stents.

As featured in:

See Martina Lenzuni, Giulia Suarato, Athanassia Athanassiou *et al.*, *Lab Chip*, 2023, **23**, 1576.

ROYAL SOCIETY OF CHEMISTRY

rsc.li/loc

Registered charity number: 207890

Lab on a Chip

PAPER

View Article Online
View Journal | View Issue

Cite this: *Lab Chip*, 2023, **23**, 1576

Dynamic investigation of zein-based degradable and hemocompatible coatings for drug-eluting stents: a microfluidic approach†

Martina Lenzuni, *[ab] Silvio Bonfadini,[c] Luigino Criante,[c] Filippo Zorzi,[cd] Maria Summa,[e] Rosalia Bertorelli,[e] Giulia Suarato ‡*[ae] and Athanassia Athanassiou‡*[a]

Biodegradable stent coatings have shown great potential in terms of delivering drugs to a damaged vessel wall, and their release profiles are key elements governing the overall performance of drug-eluting stents (DESs). However, release and degradation kinetics are usually not tested under simulated physiological conditions or in dynamic environments, both essential aspects in the design of novel DESs. To bridge this gap, fused silica-based microfluidic systems, with either round or square channel cross-sections, were designed to mimic the microenvironment of a stented vessel. In particular, we fabricated and characterized microfluidic chips based on customizable channels, which were spray-coated with a naturally-derived, rutin-loaded zein solution, to perform a comprehensive study under flow conditions. Dynamic assays after 6 hours showed how the degradation of the zein matrix was affected by the cross-sectional conformation (~69% *vs.* ~61%, square and round channel, respectively) and the simulated blood fluid components (~55%, round channel with a more viscous solution). The released amount of rutin was ~81% *vs.* ~77% and ~78% *vs.* ~74% from the square and round channels, using the less and more viscous blood-simulated fluids, respectively. Fitting the drug release data to Korsmeyer–Peppas and first-order mathematical models provided further insight into the mechanism of rutin release and coating behavior under flowing conditions. More importantly, whole blood tests with our newly developed microfluidic platforms confirmed the hemocompatibility of our zein-based coating. In detail, in-flow and static studies on the blood cell behavior showed a significant reduction of platelet adhesion (~73%) and activation (~93%) compared to the stainless-steel substrate, confirming the benefits of using such naturally-derived coatings to avoid clogging. Overall, our microfluidic designs can provide a key practical tool for assessing polymer degradation and drug release from degradable matrices under flowing conditions, thus aiding future studies on the development of hemocompatible, controlled-release coatings for DESs.

Received 5th January 2023,
Accepted 11th January 2023

DOI: 10.1039/d3lc00012e

rsc.li/loc

1. Introduction

In the past decades, drug-eluting stents (DESs) have been demonstrated to be highly effective in preventing restenosis following stenting procedures and are widely considered one of the most promising therapeutic options.[1] Since they remain in close contact with the vascular lumen and wall, DESs provide optimal delivery of the pharmacological agent(s) directly to the target region. However, an increasing body of evidence shows that anti-proliferative agents such as paclitaxel and rapamycin inhibit neointima hyperplasia but also substantially delay vascular healing and re-endothelialization.[2,3] Consequently, patients receiving DESs with the above-mentioned drugs are susceptible to thrombosis and hypersensitivity reactions (particularly in the case of rapamycin-based therapy since it suppresses immune functions).[4,5] Based on these premises, new drugs and coating technologies are being investigated, aiming at increasing the safety and efficacy of drug-eluting stents.

According to preclinical animal studies and clinical trials, the therapeutic benefits of DESs are directly reliant on their drug release kinetics, which are linked to the coating matrix

[a] *Smart Materials Group, Istituto Italiano di Tecnologia, via Morego 30, Genoa, Italy. E-mail: martina.lenzuni@iit.it, giulia.suarato@ieiit.cnr.it, athanassia.athanassiou@iit.it*
[b] *Department of Computer Science, Bioengineering, Robotics and Systems Engineering, University of Genoa, via Opera Pia 13, Genoa, Italy*
[c] *Center for Nano Science and Technology @ PoliMi, Istituto Italiano di Tecnologia, via Pascoli 70/3, Milan, Italy*
[d] *Department of Physics, Politecnico di Milano, Piazza Leonardo da Vinci, 32, Milan, Italy*
[e] *Translational Pharmacology, Istituto Italiano di Tecnologia, via Morego 30, Genoa, Italy*

† Electronic supplementary information (ESI) available. See DOI: https://doi.org/10.1039/d3lc00012e

‡ Co-last authors.

features and degradation rates, as well as the drug properties and the stent geometry.[6] With the drugs being gradually released as the polymeric coating of the stent is dissolved in the surrounding tissue, current studies are focused on tuning both the delivery of active compounds and the degradation kinetics of the matrices. Consequently, estimating these two behaviors is critical for the characterization of newly developed coating materials for DESs. Such investigation is commonly carried out under static conditions by immersing stents, or stent substitutes, in a small container with a buffer solution, periodically replaced with fresh release medium.[7] The drawback of this conventional procedure is that it does not account for the fluid dynamic environment of the DESs in the blood vessels.[6] Furthermore, this static system is not representative of the *in vivo* scenario since the saturation of the buffer with the released molecules reduces the concentration gradient between matrix components and the surrounding solution, thereby yielding erroneous release and degradation kinetics results.[7] Moreover, the composition of the elution medium may affect the delivery profiles as both drugs and polymers could be susceptible to changes in solution properties.[8] For instance, release media containing different surfactants are frequently investigated, even though many of them, such as Tween-20, could not truthfully simulate the blood components and might give inaccurate results.[9]

Blood compatibility is another major issue when evaluating DES coating materials. Surfaces with high anti-thrombotic properties, such as low platelet activation potential, are crucial for developing successful implantable medical devices.[10] Similar to the release assays, the analysis of how the composition of the coatings influences the behavior of blood components has been largely limited to static studies. On the other hand, *in vivo* experiments are expensive, time-consuming, ethically questionable, and due to their complexity, they may fail to provide detailed insight into the interactions between the coated device and the blood cells.

Recently, microfluidic technology has gained tremendous interest and opened up a new era for advanced and innovative research to simplify complex *in vivo* conditions and obtain data complementary to animal studies. With their versatile features, including small sample volume and adaptable flow conditions, lab-on-a-chip platforms offer the desirable option for conducting *in vitro* tests in a dynamic environment, recapitulating the physiological one more faithfully than experiments in conventional static cell culture dishes.[11] Moreover, microfluidic systems allow the sinking conditions around the material to be easily maintained by imposing a continuous flow inside the channels so that the released molecules can be easily dispersed into the flowing medium instead of accumulating, as in the case of a static setting, thus avoiding the effect of early leveling of the concentration gradient on elution kinetics.[12]

So far, microfluidic chambers for biomedical applications have been mostly fabricated with soft polymeric materials, in particular with the low-cost and biocompatible polydimethylsiloxane (PDMS), which can be handled to assemble user-defined shaped flow channels. However, PDMS-based devices cannot be considered fully inert (they may in fact absorb small molecules, such as hydrophobic drugs, which may cause results to be misleading), possess poor mechanical resistance and low durability (they tend to dry out or tear after a short period of time), and are difficult to reuse or recycle.[13] Some of these drawbacks could be overcome, but additional treatments and/or lipophilic coatings are necessary.[14] To overcome these limitations, in the last few years, developments in microfabrication tools (*e.g.*, femtosecond laser micromachining) in combination with novel substrate materials have offered the ability to obtain reproducible 3D microfluidic systems useful for performing microscale biochemical investigations. Femtosecond laser-assisted direct fabrication techniques can offer several advantages over standard techniques (such as soft lithography), both in terms of versatility and prototyping speed. Moreover, due to the complete freedom of the achievable 3D design, they also provide opportunities to explore new and innovative geometries, which can improve traditional microfluidic solutions.[15–17] In particular, the manufacture of 3D chips buried in fused silica is possible. This material is well known for its optical characteristics, such as transparency and low background fluorescence, gas in-permeability, thermoconductivity, high stiffness, and absolute inertness, which make it particularly unique and, at the same time, suitable for studies in the chemical and biological fields.[18] Regarding hemocompatibility studies, microfluidic platforms have been only recently investigated as potential instruments for evaluating dynamic biological interactions of desired drugs and compounds.[11,19] However, previous studies have almost exclusively focused on platelet adhesion and activation mechanisms on selected molecules, such as tissue factors and anti-thrombotic drugs, using both custom-made and commercial flow devices, as described by Provenzale *et al.*[20]

Herein, we report the design, fabrication, and validation of novel fused silica-based microfluidic platforms for investigating the hemocompatibility and dynamic behavior of drug-eluting materials for stent applications. In our previous study, we developed biodegradable DES coatings by exclusively employing biocompatible naturally-derived materials and compounds.[21] More specifically, zein, a protein derived from corn, was positively evaluated as a slow degrading carrier matrix, and rutin, a plant-derived antioxidant flavonoid, was successfully loaded as the active ingredient. Our preliminary results demonstrated excellent biocompatibility and general potential for our rutin-loaded zein (ZR) material as a DES coating. However, additional factors are involved when investigating the same composite material under dynamic flow conditions. For this reason, in the present work we aimed to reproduce as accurately as possible the physiological conditions encountered by coating materials in a patient's vasculature in the *in vitro* elution tests. In pursuit of this objective, the proposed devices comprise microfluidic channels with vessel-inspired geometry in terms of shape and dimensions. In particular, round and square

cross-sectional channels were separately constructed in order to mimic the three-dimensionalities of a partially narrowed and obstructed blood vessel, respectively. The choice of a square geometry was supported by the evidence obtained from histological images available in the literature of atherosclerotic plaques and (partially) obstructed vessels.[22–24] Each chip includes one channel coated with a rutin-loaded zein layer to examine the impact of different fluids and geometries on both the drug release and the matrix degradation kinetics. Two different release media, similar to human blood in terms of dynamic viscosity or chemical composition, were employed for comparison.

In earlier studies, Li *et al.* developed a rectangular PDMS-based channel to exclusively detect the release of fluorescent model drugs from a gold coating,[12] Jia *et al.* recently investigated the degradation characteristic of PLGA coatings with a not-well specified dynamic system,[25] while Zheng *et al.* employed a parallel plate to investigate the drug release from PLGA films under different shear stress using an aqueous Tween-20 solution as the release medium.[6] To the best of our knowledge, this work is the first one to report the deposition of a uniform, composite coating onto circular and square cross-sectional channels and to investigate its dynamic behavior in terms of drug release and matrix degradation in the presence of simulated blood fluids for DES application. Moreover, this work is intended to provide a simple and versatile platform to gain insights into the complex dynamic interactions between degradable coatings and blood components in stented arteries for the successful design of highly efficient and hemocompatible DESs.

2. Experimental

2.1 Materials

Pure zein powder, rutin hydrate, urea, glycerol, sodium chloride, sodium bicarbonate, potassium chloride, sodium phosphate dibasic, magnesium chloride, calcium chloride, sodium sulphate, heparin sodium salt, Trizma® hydrochloride, hydrochloric acid, and 5 μm-diameter polystyrene (PS) beads were provided by Sigma-Aldrich (St. Louis, USA) and used as received without further purification. Waterborne polyurethane, grade ICO-THANE 10, was provided by I-Coats NV (Berchem, Belgium). Polylactic acid 6060D was purchased from Nature Works LLC (Minnetonka, USA). UV photocurable glue "NOA63" was purchased from Norland Products (Cranbury, USA). Commercial stainless steel flat sheets (316L SS, 500 mm × 300 mm × 0.5 mm) were purchased from RS Component (Milan, Italy). Dulbecco's phosphate buffered saline (PBS), dimethyl sulfoxide (DMSO), dichloromethane (DCM), ethyl acetate, and ethanol (≥99.8%) were purchased from Sigma-Aldrich (St. Louis, USA), while deionized water (ddH_2O) was supplied by a Milli-Q Integral purification system (Millipore, Bedford, USA).

2.2 Design and fabrication of the microfluidic devices

The ability to mimic the *in vivo* topography of complex biological systems may offer several critical advantages, leading to results that can closely resemble *in vivo* observations. The lab-on-a-chip platform can be used as a versatile primary strategy to achieve a holistic picture of cardiovascular problems, especially when manufactured into non-deformable and completely inert substrates such as fused silica. Here, we worked towards the realization of *ad hoc* designed microfluidic devices to mimic key flow dynamic properties of a stented artery. As previously mentioned, the case of atherosclerotic plaques that severely occlude an artery is modelled with a square cross-sectional channel, while a round cross-section was chosen to replicate a partially occluded stented artery. To fabricate the aforementioned chips, we exploited femtosecond (fs)-laser-assisted micromachining in combination with a wet etching process (FLICE: femtosecond laser irradiation followed by chemical etching) due to its ability to quickly realize 3D structures without the requirement of masks or a clean room. The peculiar manufacturing process is composed of two main steps (Fig. 1(a)). In the first step, an ultrashort-pulsed laser beam, following the 3D-designed geometry, irradiates a fused silica substrate. Thanks to non-linear absorption effects, the chemical–physical properties of the material are modified only in the region confined in the beam spot volume. The second step – wet etching – consists of an ultrasonic bath in a chemical solution (20% aqueous hydrofluoric acid (HF)) that allows the selective removal of the modified material to create the specific 3D geometry. The writing parameters were carefully set to create a permanent bulk modification: the chemical bonds between silica and oxygen atoms are broken, and the appearance of unique nanostructures – known as nanogratings or nanocracks (Fig. 1(a)) – occurs. These self-assembled, periodic structures show an alternation of high- and low-density material oriented perpendicular to the laser beam writing polarisation, promoting the access of the etchant solution to the material to be removed, improving the reaction products' diffusion. Thus, selective material removal is possible, allowing the creation of 3D structures. The laser micromachining setup is composed of a 10 W amplified femtosecond laser source (Pharos-Light Conversion), an external harmonic generator (HIRO-Light Conversion), and an optical setup with which every writing parameter (power, polarization, wavelength, fluence, *etc.*) can be controlled. The characteristics of the laser source are: pulse duration of 240 fs, a fundamental wavelength of 1030 nm, and a repetition rate ranging from 1 kHz up to 1 MHz. The fused silica irradiation was achieved using the second harmonic laser line (515 nm) with a 500 kHz repetition rate and an average power of 200 mW. The pulsed laser beam was focused on the sample with an achromatic objective (40×, N.A. 0.4, Mitutoyo, Kawasaki, Japan). Samples were placed on computer-controlled 3-axis high-resolution (<50 nm) air-bearing translation stages (ABL-1000, Aerotech, Pittsburgh, USA).

With the aim of functionalizing the inner surfaces of the channels with zein coatings, as is reported in paragraph 2.3, the unique geometry chosen involved fabricating two open chip sections (Fig. 1(b and c)) instead of a single buried one and then sealing them with a transparent and removable

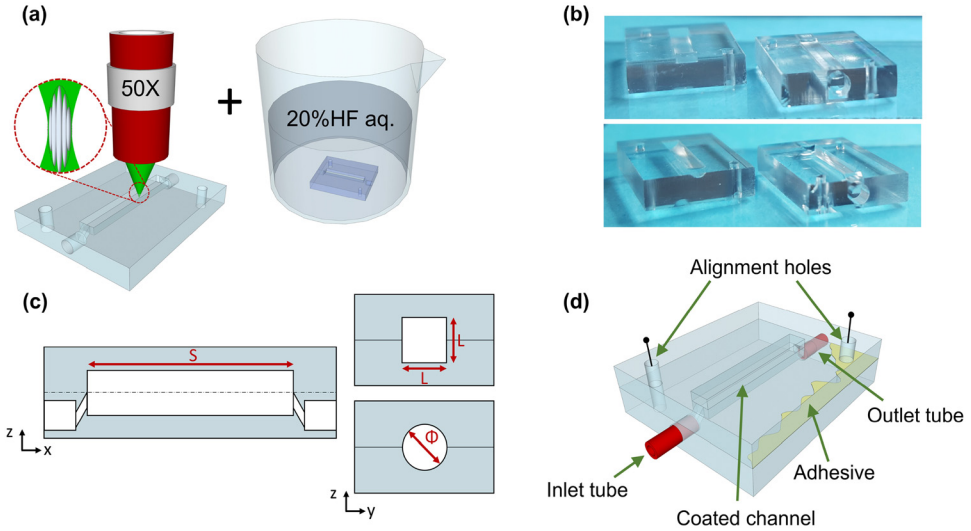

Fig. 1 Microfluidic device design. Illustration of the two steps of the FLICE fabrication method of fused silica-based microfluidic devices. Ultrashort pulse laser induces the nanogratings (or nanocracks) formation, as visually highlighted in the spot zoom inset, which are useful for the chemical etching process (a). Bright-field microscopy photographs of the disassembled microfluidic devices (b). Schematic diagram of the microfluidic chip structures along the *z*–*x* and *z*–*y* planes (c), and a 3D schematic of the assembled device (d), which shows the fluid inlet and outlet tube accesses and the alignment holes.

optical adhesive (Fig. 1(d)). In this way, the two sections could be independently handled, reviewed, analyzed, and then stacked and aligned so that the same device could be used multiple times. The fabricated microfluidic chip dimensions were 9.8 mm (width) × 13.9 mm (length) × 2.8 mm (height). The round channel consisted of a gap with a circular opening in the middle (diameter = 1.8 mm), while the square one consisted of an opening of 1.8 × 1.8 mm^2. The geometry is complemented by two access points, buried at the bottom of the chip, for the integration of tubes (inlet and outlet) connected with the outside environment (Fig. 1(d)). The entire longitudinal distance between the inlet and outlet holes of the device was 10 mm.

2.3 Fabrication and characterization of the zein-based coated-channels

A rutin-loaded zein (ZR) solution was prepared by dissolving rutin powder in 5% v/v DMSO and then diluting it with a mixture of ethanol (76% v/v) and deionized water. Afterwards, zein powder was added to form a final solution of 15% w/v zein and rutin (10% w/w_{zein}). The mixture was stirred at room temperature at a mixing speed of 700 rpm for 60 minutes until complete dissolution. The ZR solution was sprayed for 6 seconds at a distance of 30 cm on each pair of open sections (lower and upper chambers) of the microfluidic chips using an airbrush spray coating system (0.55 mm nozzle diameter, model VL-SET, Paasche Airbrush Company, Chicago, USA). The coated chambers were allowed to dry overnight at room temperature. The weight of the sprayed coating can be obtained by subtracting the weight of the empty chip from the weight of the coated chip. By comparing this result with the weight of 1 mL of dried ZR solution, the amount of zein and/or rutin deposited on each chip can be estimated. The surface morphologies and thicknesses of the polymer coatings were observed by scanning electron microscopy (SEM) using a SEM JSM-6490LA microscope (JEOL Inc., Peabody, USA) at 10 kV accelerating voltage. The chemical structures of the coatings were thoroughly characterized by Fourier transform infrared (FTIR) and X-ray photoelectron (XPS) spectroscopy in our previous study.[21] A scratch was manually performed onto the coated chambers using a lancet, and the thickness values of the polymer layer were confirmed using a surface profilometer (Ambios XP-2, Ambiostech, Santa Cruz, USA) equipped with a diamond-tipped stylus (radius = 2 μm), which acted across the surfaces under a constant load of 0.5 mN with a speed of 0.5 mm s^{-1}. Similar parameters were used to obtain the average roughness values of the ZR-coated channels. In order to study the surface wettability, the ZR solution was sprayed on the flat area of the chambers, following the same operational parameters; contact angle measurements were then conducted with a contact angle goniometer (Dataphysics OCA 20, Filderstadt, Germany). Briefly, by means of a sessile drop method, 5 μL drops of ddH_2O were deposited onto 10 different surface spots with a microsyringe, and the acquired images were elaborated using the SCA20 Software (Data Physics Instruments GmbH, Filderstadt, Germany). The angle between the baseline of the drop and the tangent at the drop boundary was determined, and the resulting contact angle measurements were calculated by taking the arithmetic average of the left and right contact angles of each droplet.

2.4 Preparation of simulated blood fluids (SBFs)

The choice of suitable release media is an important aspect while studying the behavior of biomedical coating

materials. In this study, two types of simulated blood solutions were prepared:

- SBF_wgu identifies a mixture of water, glycerol, and urea, and solutions with different mixing ratios were prepared with the aim of obtaining a fluid that could match the dynamic viscosity of human blood ($\mu \sim 4$ mPa s).[26] In particular, three ratios of water, glycerol, and urea were chosen and tested, as reported in Fig. S1(a) and Table S1.† These mixtures were allowed to stir at room temperature for 12 hours, and, subsequently, rheological properties were measured with a Haake Mars 40 rheometer (Thermo-Scientific, Karlsruhe, Germany) equipped with a conical probe C60 1°/Ti. Dynamic viscosity values were obtained through a shear rate sweep (shear rate $\approx$ 0.1–1000 s^{-1}) while the temperature was kept constant at 25 °C.
- SBF_ws indicates an aqueous mixture to which various salts were added to create a fluid whose ion concentrations are nearly equal to those of human blood plasma. SBF_ws was prepared according to a protocol previously described.[27] The reagents were dissolved one by one in deionized water at 37 °C with a magnetic stir bar in the order given in Table S2,† where the SBF_ws composition is reported. A digital pH-meter (HANNA HI2002, Hanna Instruments, Rhode Island, USA) was used to adjust the pH of the resulting solution to 7.4 to match the blood physiological pH.

2.5 Microfluidic platform assembly and in-flow experimental procedure

In order to ensure a leak-free coupling between the two coated sections of each microfluidic chip, UV-curable NOA63 was applied along the perimeter of the chambers before closing. To ensure that, after the sealing operation, the microfluidic chamber always presented the same nominal 3D geometry as designed, the top and bottom sections were systematically aligned by means of references. Guide holes, superimposed on a pivot, ensured the perfect alignment of the chambers, comparable to that of a single monolithic device, as shown in Fig. 1(d). To increase the system stability, the sealed microfluidic chips were bonded to a standard glass microscope slide with a small amount of NOA63. A UVGL 58 lamp (UVP, Upland, USA) emitting at 365 nm was used to polymerize the adhesive. The microfluidic setup was assembled with 1/16″ OD × 0.02″ ID perfluoroalkoxy (PFA) tubes (IDEX Health&Science, Oak Harbor, USA), sealed with NOA63 at the inlet and outlet ports of each chip. The device was perfused with fresh medium at a controlled flow rate by a LiveFlow peristaltic pump (IVTech, Massarosa, Italy) joined to the inlet tube *via* Luer adapters, and the elution medium was introduced from the SBF-filled reservoir to the pump tubes. To simulate the *in vivo* conditions of a cardiovascular stented artery, all the experiments were conducted with a continuous flow rate of 500 μL min^{-1} at 37 °C. The set flow rate was in the range of the blood flow calculated for the diameter of our vessel-mimicking devices.[28] The physiological temperature was maintained by heating the SBF-filled reservoir on a hot plate. After passing through the microfluidic channel, the eluted medium was dropped into collection tubes and stored prior to analysis. A photograph of the assembled microfluidic system can be seen in Fig. 2(b).

2.6 Three-dimensional computational fluid dynamic (CFD)

To investigate the flow environment of the microfluidic channels in the fabricated devices, fluid dynamics analyses were performed based on computational models developed in COMSOL Multiphysics 5.3 (Burlington, USA). The fluid characteristics and boundary conditions in the numerical model were specified to mimic the experimental setup. As a balance between computational cost and spatial resolution accuracy, a dynamic mesh volume length was used: less closely packed in the secondary section (pipes, inlets, fittings) and denser in the central section of greatest interest. The complete fluid dynamic field was obtained by solving the Navier–Stokes and laminar flow equations. Considering that the two proposed SBFs show similar densities values (1.03 g cm^{-3} for SBF_ws and 1.15 g cm^{-3} for SBF_wgu), the longitudinal and transversal velocity distributions were determined by imposing the SBF_wgu flow inside the channels with the previously mentioned flow rate and viscosity (Table S1†).

2.7 Matrix degradation studies

The degradation rate of the zein matrices may not only depend on their own intrinsic properties but also on other factors, including the diffusion dynamics of materials, the degradation media composition, environment-dependent forces, and the coating geometry. In order to investigate the degradation kinetics of our zein-based polymeric coatings deposited onto the microfluidic channels under flow conditions, every SBF prepared was perfused into the round and square devices as the elution medium for up to 6 hours. At fixed time points (ranging from 15 minutes to 6 hours), the media were withdrawn for analysis, and fresh SBF was immediately replenished into the heated reservoir. Absorbance at 270 nm (zein λ_{max}) was determined for each sample with a Cary 6000i UV-vis-NIR spectrophotometer (Varian, Palo Alto, USA). The amount of zein released at each time point was calculated by an appropriate calibration curve, and the results were expressed as the percent of cumulative zein degraded over time according to eqn (1).

$$\text{Cumulative amount of degraded zein (\%)} = \frac{\text{Mass of zein into the eluted medium (at time} = t)}{\text{Total mass of zein on the channel (at time} = 0)} \times 100 \quad (1)$$

In order to assess the presence of surface morphological changes during the dynamic flow experiments, at specific time points the microfluidic chips were quickly rinsed with deionized water to eliminate any residual salt, opened by removing the adhesive with gentle swabbing of DCM, and left

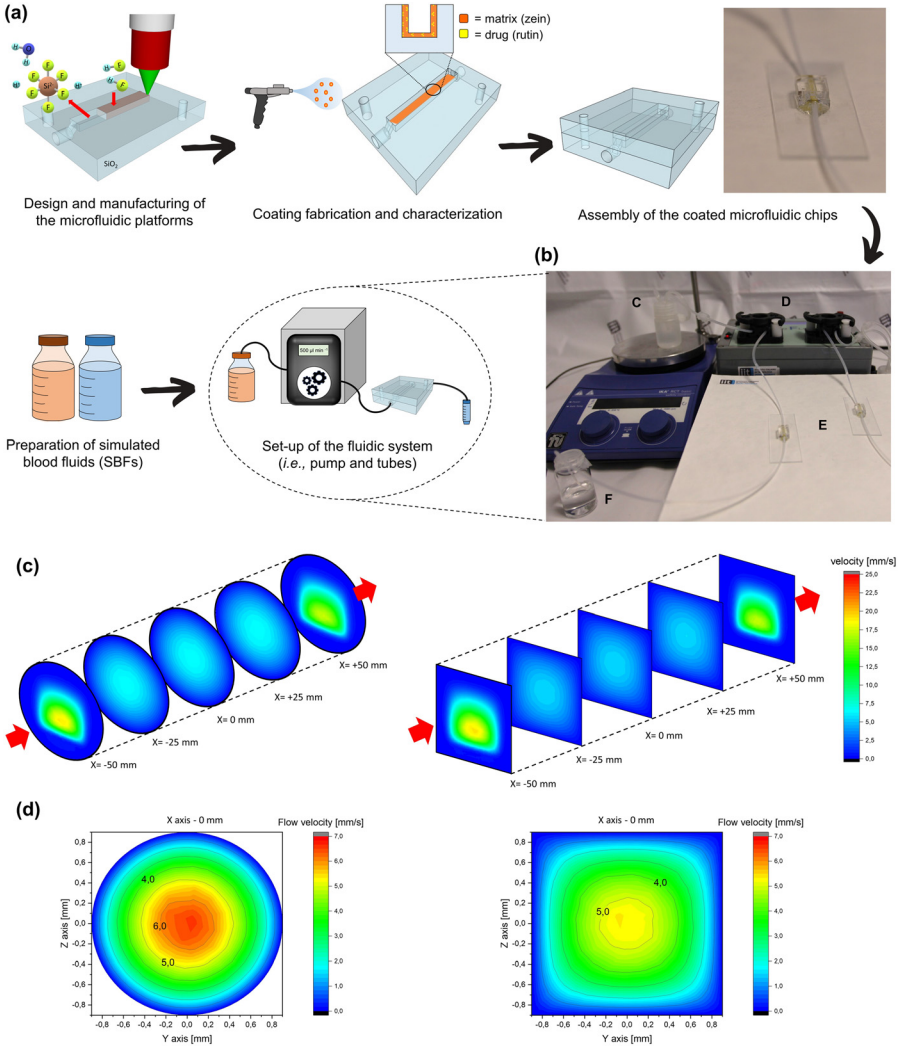

Fig. 2 Schematic illustration of the fabrication process, setup of the microfluidic system, and CFD analyses. (a) Once the chips were fabricated, the zein-based solution was sprayed on the disassembled chambers and the resulting coating was characterized. The chips were then assembled and connected with inlet and outlet tubes. (b) Photograph of the assembled microfluidic device and experimental setup, comprising a heated reservoir containing a SBF (C), a peristaltic pump (D), the device (E), and an outlet container (F). Parallel assays can be performed simultaneously for different chip geometries or different SBF formulations. Simulated blood fluid flow velocity distributions through the whole channels (c) and central *y*–*z* cross-section (d) of the microfluidic devices were modeled using COMSOL Multiphysics, with the colors indicating the local velocity rate. Simulations were performed at 500 μL min^{-1}.

to air-dry. The morphological features of the degraded coatings (surface and cross-section) were observed under the SEM. Differences in the degradation kinetics and morphological behaviors between microfluidic chips of different cross-section geometry resulting from the elution of different fluids were studied and compared.

2.8 Drug release kinetics and mathematical models

The collected samples described in paragraph 2.7 were analyzed in order to determine the concentration of the active compound (rutin) released in the elution media at each time point. The absorbance at 362 nm (rutin λ_{max}) was recorded, and results were expressed as the cumulative percent of rutin released over time according to eqn (2).

$$\text{Cumulative amount of released rutin (\%)} = \frac{\text{Mass of rutin into the eluted medium (at time} = t)}{\text{Total mass of rutin on the channel (at time} = 0)} \times 100 \quad (2)$$

The influence of either the channel geometry or the elution media on the drug release profiles was studied and compared. Moreover, the percentage of cumulative drug release during the experiment was analyzed on the basis of various mathematical models. In particular, several commonly used power-law equations were employed to fit rutin release rates and helped to explain the underlying transport mechanisms. Between the main drug release kinetic models, zero-order, first-order, Higuchi, Hixson–Crowell, and Korsmeyer–Peppas models were applied and

compared.[29] The highest correlation coefficient (r^2) values indicate the most accurate and best-fitted kinetics models to describe the occurring drug release mechanisms.

2.9 Polystyrene beads-containing SBF dynamic experiments

A first proof-of-concept experiment was carried out using 5 μm-diameter polystyrene (PS) beads as a cell model, as already reported in the literature.[30] In order to mimic the effect of red blood cells (RBCs, *i.e.*, 99% of the cellular component of blood) and particulated blood fluids, the PS beads were suspended in the previously prepared SBFs to a final concentration of 5×10^6 beads per mL. Zeta potential recordings of diluted PS beads were acquired *via* dynamic light scattering (DLS) using a Zetasizer Nanoseries (Malvern Instruments, Worcestershire, United Kingdom). Three measurements were averaged for each sample. Under the same conditions described in paragraph 2.5, freshly prepared SBF solutions loaded with PS beads were flowed through the microfluidic devices for 30 minutes. The fused silica-based chips were then carefully opened by removing the adhesive, sputter-coated with 15 nm gold, and SEM analysis was immediately performed to investigate the possible bead adhesion and the resulting ZR coating morphology.

2.10 Hemocompatibility tests

Hemocompatibility tests were performed to determine the blood compatibility of the proposed zein-based coatings for stent application. As reported in the literature, the most critical phase during blood coagulation and thrombus formation on artificial surfaces is platelet attachment.[31] Since the physical presence of red blood cells is known to have a significant impact on platelet adhesion, whole blood assays comprising both platelets and RBCs were carried out.[32] In particular, static and dynamic experiments of whole blood cell adhesion onto coated surfaces were performed and compared. Regarding the blood-related experiments, male C57BL/6 mice weighing 22–24 g were used (Charles River, Calco, Italy). All procedures were performed in accordance with the Ethical Guidelines of the European Communities Council (Directive 2010/63/EU of 22 September 2010) and accepted by the Italian Ministry of Health. All efforts were made to minimize animal suffering and to use the minimal number of animals required to produce reliable results, according to the "3Rs concept". Animals were group-housed in ventilated cages and had free access to food and water. They were maintained under a 12 hours light/dark cycle (lights on at 8:00 am) at a controlled temperature (21 ± 1 °C) and relative humidity (55 ± 10%). Specifically, native whole blood was collected from naive mice in vacutainer tubes containing heparin (5000 U mL^{-1}) according to ISO 10993 norm and standard practices for flow assays.[33–36] Whole blood was immediately diluted with normal saline (4 : 5 v/v) and used within 2 hours of collection.

2.10.1. Blood cell adhesion and hemolysis assays. Static conditions were used to test and compare several coating materials deposited onto 316L SS flat samples (1.8 × 1.8 cm^2 exposure area). In particular, in addition to our fabricated zein-based coatings, with and without rutin, reference materials such as polyurethane (PU, dissolved in water) and polylactic acid (PLA, dissolved in ethyl acetate) were used as coating polymers for comparative purposes. For the static blood cells adhesion assay, a 200 μL drop of diluted whole blood was placed on each sample and incubated for 30 minutes at 37 °C, according to the scientific literature.[37,38] Samples were then rinsed three times (5 minutes each) with PBS to remove the non-specifically adsorbed cells. The remaining adherent platelets and RBCs were immediately fixed with 2% glutaraldehyde in 0.1 M sodium cacodylate buffer (pH 7.4, Sigma Aldrich) for 90 minutes at room temperature. The fixative solution was subsequently withdrawn, and the samples were washed three times for 10 minutes each with 0.1 M sodium cacodylate buffer and stored overnight at 4 °C. The samples were post-fixed in 1% osmium tetroxide (Sigma Aldrich) in 0.1 M sodium cacodylate buffer and then dehydrated in a series of ethanol solutions. Finally, they were incubated in hexamethyldisilazane (HMDS, Sigma Aldrich)/ethanol solution series, air-dried, sputter-coated with 15 nm gold in order to avoid charging effects, and were analyzed by SEM. Platelet density was quantified from the acquired micrographs using an image analysis software program (ImageJ, Wayne Rasband, NIH, **https://rsbweb.nih.gov/ij/**), and results were expressed as the average number of adherent and activated platelets per mm^2. The development of platelet filopodia is the first morphological alteration linked with activation and aggregation. These processes are thought to help platelets to bind to other platelets and produce fibrin strands. Activated platelets, easily detected by the presence of filopodia, were manually distinguished in SEM images from resting platelets, the latter showing a spherical structure with no filopodium extending from the body of the platelet.[39–41]

According to the international standard ISO 10993-4, the hemolysis assay was performed for the same coating materials and reference samples.[36] Briefly, samples with a 1.8 × 1.8 cm^2 exposure area were soaked in 2 mL of normal physiological saline and kept at 37 °C for 30 minutes. Subsequently, 0.04 mL of diluted blood was added, and the samples were kept at 37 °C for additional 60 minutes. Normal physiological saline and distilled water served as negative and positive controls. Lastly, the solutions were withdrawn and centrifuged at 3000 rpm for 10 minutes at room temperature. The absorbance (Abs) of the supernatant (~100 μL) was measured at 542 nm using a Spark Multimode microplate reader (Tecan Group Ltd., Männedorf, Switzerland). The hemolysis rate (HR) was calculated according to eqn (3).

$$\mathrm{HR}\ (\%) = \frac{\text{Sample Abs} - \text{Negative control Abs}}{\text{Positive control Abs} - \text{Negative control Abs}} \times 100 \quad (3)$$

2.10.2. Dynamic hemocompatibility experiments. The dynamic flow experiments were performed using a peristaltic

pump at a continuous flow rate of 500 μL min^{-1}. Before the assay, the assembled microfluidic chips were perfused with PBS and checked for the absence of air bubbles or fluid leakage. Whole blood samples (*ca.* 1.5 ml each) were then drawn through the tubing system into the microfluidic devices, and the flow was sustained for 10 minutes, after which the devices were rinsed with pre-warmed PBS in order to remove unbound platelets and RBCs within the coated channels. Afterwards, the microfluidic platforms were carefully disassembled, and the adherent cells on the coatings were immediately fixed, as mentioned above. SEM analysis was performed on randomly chosen areas to investigate blood cell adhesion, platelet morphology, aggregation, and filopodia formation (as a sign of activation). Additionally, the acquired images were analyzed to quantify the area covered by platelets with an image analysis software program.

2.11 Statistical methods

All the measurements were statistically analyzed with Origin 2019 software (OriginLab Corporation, Northampton, USA). To identify statistically significant differences between two groups, an unpaired Student's *t*-test was used. A one-way ANOVA followed by Tukey's test for post-test comparisons was used when more than two groups were compared. Probability values of $p < 0.05$ (*) and $p < 0.01$ (**) were considered statistically significant.

3. Results and discussion

3.1 Microfluidic system setup and three-dimensional computational fluid dynamics

The pioneering study of drug release and matrix degradation under flow conditions, exploiting our microfluidic platform, enabled the performance of a series of analyses repeatedly, and at regular intervals, directly on the fluidic channel coating. It is also important to emphasize that the transparency of the material was a fundamental property required for the fabrication technique and the operation of the devices, *i.e.*, opening the chips, applying the coatings, and closing the chips with UV-curable glue. Fig. 1(b) shows the resulting microfluidic platforms that consist of two asymmetric halves that have been assembled, as shown in Fig. 1(d), with adhesive glue. Two device configurations were prepared with round and square cross-sectional channels in order to compare the effect of the geometric parameters while mimicking the small arteries' profiles in partially and severely obstructed conditions (*i.e.*, clogged stented artery).

The working fluids detailed in Fig. S1† were prepared as blood analogs. Simulated blood fluid "ws" was prepared in accordance with the ion chemical composition of human blood (Table S2†). Moreover, during the initial stage of this work, several release media containing different water, glycerol, and urea concentrations were investigated. Table S1† summarizes the final properties of all two- and three-component "wgu" solutions. On the basis of the preliminary results (Fig. S1(a)†), a release medium containing 32.8% w/w glycerol and 22.4% w/w urea was selected as especially suited for our application and employed in all the following studies. In particular, both the dynamic viscosity (4.1 mPa s) and pH value (7.3) were more similar to the desired physiological conditions compared to other fluids reported in the literature to date that are commonly employed in degradation and/or release experiments.

Fig. 2(a) illustrates the setup steps of the microfluidic devices, while the final system adopted for our experiments, presented in Fig. 2(b), comprised the peristaltic pump, the device, the outlet collector vials, and a heated reservoir containing the SBF. Alternatively, the chips and the whole system could be placed in incubators and eventually used to investigate stimuli-responsive materials by imposing external triggers. The fused silica-based chips were also extremely durable, allowing for repeated cleaning and recycling processes. Here the intention was not only to recapitulate the blood circulation within a stented artery but also to recreate a constant, physiological concentration gradient between the coated surfaces and the flowing eluting medium. Computational fluid dynamics (COMSOL Multiphysics package/ANSYS) was used to calculate the hydrodynamic field behaviors in both our microfluidic devices. The simulation of the local flow environments is represented as a series of vertical cross-sections, as shown in Fig. 2(c). Although there are no noteworthy differences in the fluid dynamics behavior between the circular and square channels in the central area of interest, with a closer look Fig. 2(d) shows the following. In the first 100–150 μm from the walls towards the center of the channel, the velocity field of the fluid is almost zero (semi-stationary bearing effect). This is not a surprising feature in a microfluidic study; however, considering a thickness of about 6–7 μm of the polymer matrix incorporating the drug, it is safe to assume that the degradation and drug release processes are mainly driven by an unforced diffusion mechanism or an erosion mechanism, which is based on the biochemical affinities and/or the concentration gradients of the various species (as reported in paragraphs 3.3 and 3.4). Specifically, the active molecule diffuses in the fluid, reaches the most central flow lines, and is transported toward the exit. Continuous exchange with a new solution medium (as occurs in the human body) prevents saturation conditions from being reached, recreating the initial concentration conditions that facilitate the release process.

3.2 Characterization of the zein-based coated channels

Fig. 3 shows the surface morphologies of the ZR-coated channels. After the spray coating with the ZR solution, the channel surface became rougher than the bare substrate obtained with the FLICE fabrication procedure, as visible in Fig. 3(d). In order to ensure maximum adhesion of the polymeric composite to the fused silica, the surfaces of the channels were not smoothed down to optical quality. From the SEM observation, the chambers appear uniformly coated and free from cracks (Fig. 3(a and b)). Various magnifications highlight how the coating is deposited in a relatively

homogenous way from the bottom to the edges of the channels, thus nicely replicating a uniformly-coated drug-eluting stent adhering to a vessel wall. This aspect is of particular importance since coating homogeneity is crucial in order to guarantee a uniform drug delivery to the diseased vessel segment and to decrease therapeutic risks.[42,43] The coated surfaces were scanned with a stylus profilometer, and similar roughness values were extrapolated for the round and square cross-section chambers (Table 1). The thickness of the coating at the bottom of each channel was examined with the same instrument after the samples were intentionally scratched with a scalpel. Similar coating thickness values were found on the round and square cross-section chambers, as shown in Table 1. These measures are comparable to those obtained by analyzing SEM cross-sectional images, and, in particular, a medium value of 7.2 μm was calculated from Fig. 3(c) *via* ImageJ. Finally, the surface wettability of the coated substrates was characterized based on the water contact angle measurements. Experimental results revealed that ZR-coated chambers were partially hydrophilic as they display a mean water contact angle of 60.5° (Table 1), which is in accordance with the previously obtained values for zein-based substrates.[21,44]

3.3 Matrix degradation studies

Zein is a protein-based natural polymer still little investigated for its biomedical applications but has already shown a slow degradation rate in aqueous environments, especially compared to other naturally-derived polymers.[21,45,46] To investigate the degradation kinetics of the polymer composite coating under dynamic conditions, the ZR-coated channels were exposed to two aqueous SBFs at a continuous flow rate of 500 μL min^{-1} for up to 6 hours. In the first stage of the degradation kinetics, the polymer release appears more abrupt, while the zein mass remaining on the channels continues to decrease at the following stages but at slower rates, consequently diffusing into the release media (Fig. 4). The composition of the working fluids used for the experiments affects the overall polymer degradation: more specifically, in our case, a difference in the zein release profiles was observed within the first hour for round cross-section channels (34.5 ± 3.2% with SBF_ws and 23.1 ± 2.5% with SBF_wgu, Fig. 4(a)) and square cross-section channels (38.6 ± 2.9% with SBF_ws and 33.7 ± 4.9% with SBF_wgu, Fig. 4(b)). It is particularly noteworthy that the use of SBF_ws could lead to the creation of more leachable zein fragments at an earlier time, resulting in a faster film mass loss. As already suggested in the literature, an increase in the percentage of salts in the flowing medium might catalyze the hydrolysis reactions and may be the major cause of this fragment release increase.[47,48] Moreover, it has to be noted that SBF_wgu not only presents a lower salt concentration but, being more viscous than SBF_ws (Table S1†), it is characterized by a higher streaming resistance, thus flowing slower through the channel. When the flow rate is reduced, the degradation rate may likewise decrease, resulting in longer degradation times for the coated samples.[49] Furthermore, the presence of glycerol in

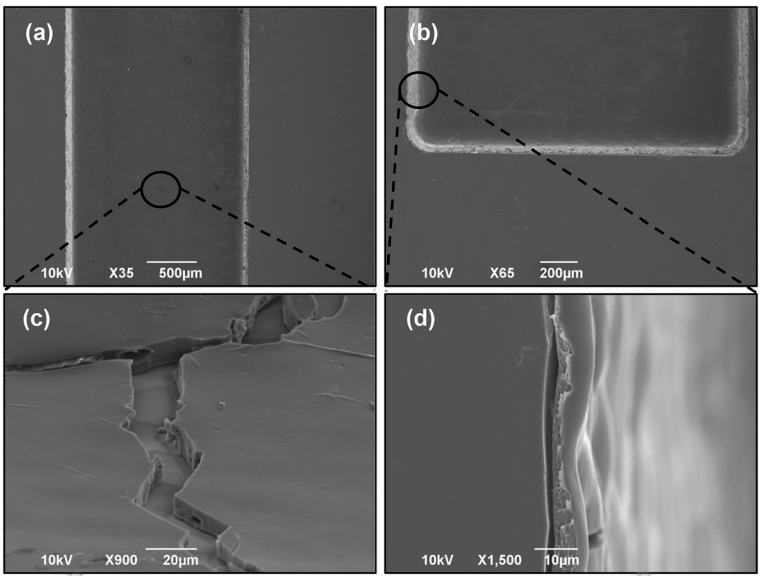

Fig. 3 Characterization of the coated channels. Morphological characterization showing SEM images of surfaces (a and b) and cross-section (d) of the square channel. (c) SEM image of the bottom of a coated channel after being scratched.

Table 1 Physico-chemical properties

Coating material	Water contact angle (°)	Coating thickness (μm)	Arithmetic roughness (nm)
Rutin-loaded Zein (ZR)	60.5 ± 2.6	6.6 ± 0.5 (square channel) 7.5 ± 0.2 (round channel)	403.0 ± 74.6 (square channel) 438.5 ± 54.9 (round channel)

SBF_wgu might be responsible for a lower zein degradation kinetics over the 6-hour time period (round channel: 55.0 ± 6.6%; square channel: 60.9 ± 4.8%): this plasticizer molecule not only increases the viscosity of the aqueous layer at the fluid–coating interface but also may limit the swelling of the polymeric film. Consequently, the initial fragments and later zein diffusion through this glycerol-rich aqueous layer becomes more difficult, and the resistance to polymer erosion may rise.[50]

As shown in Fig. 4(a) and (b), the initial "burst effect" in the delivery kinetics is slightly faster for the square cross-section channel (*e.g.*, after 30 minutes, SBF_ws: 29.8 ± 3.6%, SBF_wgu: 25.0 ± 5.6%) compared to the round cross-section one (SBF_ws: 28.1 ± 3.1%; SBF_wgu: 16.7 ± 1.3%). This small difference can be attributed to the square channel geometry, which resulted in a higher exposed area of the polymer matrix to the flow of the release medium. Overall, it can be concluded that the degradation of the zein coatings is plausibly due to the direct penetration of the water molecules of the release media into the films, causing random breakage of the zein amide bonds.

Changes in the surface morphology of the zein-coated channels were observed under the SEM after dynamic tests were performed at several time points, and the results are shown in Fig. 5 and S2.† Zein-based coatings presented a uniform, compact surface at time t = 0 (Fig. 3), while degradation signs were visible at all the other time points. In

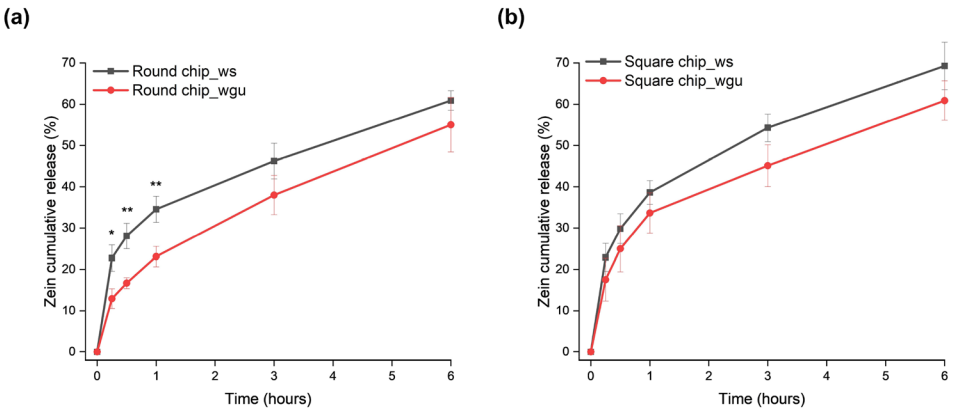

Fig. 4 Zein matrix degradation kinetics. Cumulative percentage of zein mass released from round (a) and square (b) ZR-coated channels. All experiments with different simulated blood fluids (water/salts "ws" or water/glycerol/urea "wgu") were conducted at 37 °C. Data are presented as mean ± SD (n = 3), which were statistically analyzed using Student's t-test. * $p < 0.05$, ** $p < 0.01$.

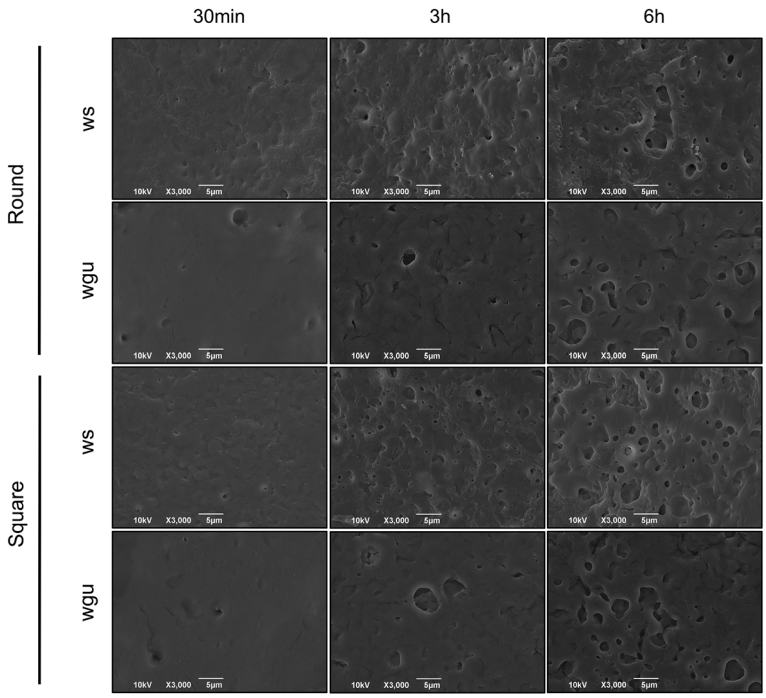

Fig. 5 SEM morphologies obtained from the coated channels over time. Morphological changes were observed on the bottom of the coated channels during the degradation process. Representative SEM images of the square and round chips were taken at different time points (from 30 minutes to 6 hours).

particular, the samples exhibited an increasing porous surface over time as the release media flowed. By performing a qualitative analysis comparing the SEM images of the coated channels after exposure to the two fluids under study, SBF_ws appears to be a more aggressive and erosive fluid than SBF_wgu since the pore surface areas are larger in the samples subjected to the first fluid flow. These results are in accordance with those previously presented in Fig. 4, showing the eluted samples' concentrations studied with the spectrophotometer. On the other hand, surface topographical variations were not identified when the different channel geometries were compared (Fig. 5 and S2(a)†), which confirms the previous non-statistically different degradation data reported in Fig. 4. Cross-sections were also inspected by SEM: the residual coating thickness appeared to gradually diminish over time (Fig. S2(b)†); nevertheless, after 6 hours of flow, the zein layer still uniformly covered the underlying fused silica-based substrate.

Overall, the degradation products did not peel off as large fragments and did not emerge as cracked pieces, indicating an optimal degradation behavior of the zein matrix and good adhesion between the coating and the substrate. As previously explained in paragraph 3.2, these results confirm that the surface roughness of the microfluidic channels, generated with the FLICE fabrication technique, offers an important contribution to the polymer adhesion strength. As a further confirmation, the zein absorption peaks (270 nm) observed in the UV spectrophotometer were generally represented as well-defined curves and, in the spectra region around 320 nm, which is usually associated with protein aggregation, no broad peaks were observed (data not shown).

3.4 Drug release kinetics and mathematical models

Rutin release from the zein-coated channels was tested for 6 hours in the two microfluidic devices by flowing SBF_ws and SBF_wgu at 37 °C. The effect of the eluting media composition on the release rate of rutin is shown in Fig. 6, where the cumulative percentage of drug released is plotted as a function of time. After 6 hours, the released amounts of rutin into the SBF_ws fluid from the round and square microfluidic chips were 77.0 ± 6.9% and 80.8 ± 7.2%, respectively. Values of 73.8 ± 4.5% and 78.1 ± 8.5% were obtained for the round and square channels, respectively, when using SBF_wgu. No statistically important differences were observed between the amounts of drug released in the two fluids and within the channels with different geometries. To gain a comprehensive understanding of the drug–polymer interaction, the release profiles of both zein and rutin from each type of channel with the two different elution media were compared and are shown in Fig. S3.† At the initial stages of the process (15–30 minutes), we observed an initial release of both rutin and zein. Afterwards, the drug release appears to occur more rapidly than the polymer degradation process, assuming that at this point the rutin release kinetics is mainly driven by diffusion mechanisms. To get further insight into the underlying drug release mechanisms, mathematical models were used alongside release kinetics studies.[29] In particular, the cumulative release profiles were fitted to the theoretical equations presented in paragraph 2.8. As reported in Table 2, the most accurate models for the mathematical description of rutin delivery kinetics are the Korsmeyer–Peppas (Fig. S4(a and b)†) and the first-order model (Fig. S4(c and d)†). r^2 values, *i.e.*, the goodness-of-fit measure, are given in Table 2 for all the samples. According to the n coefficients (namely the release exponents of the Korsmeyer–Peppas model), which lay below 0.5 for both configurations and both fluid conditions, drug release from zein matrices is thought to occur through the partially swollen zein matrix and to be mainly controlled by a Fickian type diffusion (*i.e.*, the diffusion rate of the penetrating solvent is much greater than the relaxation and degradation rate of the polymeric chains), as already suggested by the comparisons shown in Fig. S3.†[29,51] Further insight into the release mechanism is obtained by analyzing separately two regions of the release curves (Table S3†). For the first time period up to 1 hour, the

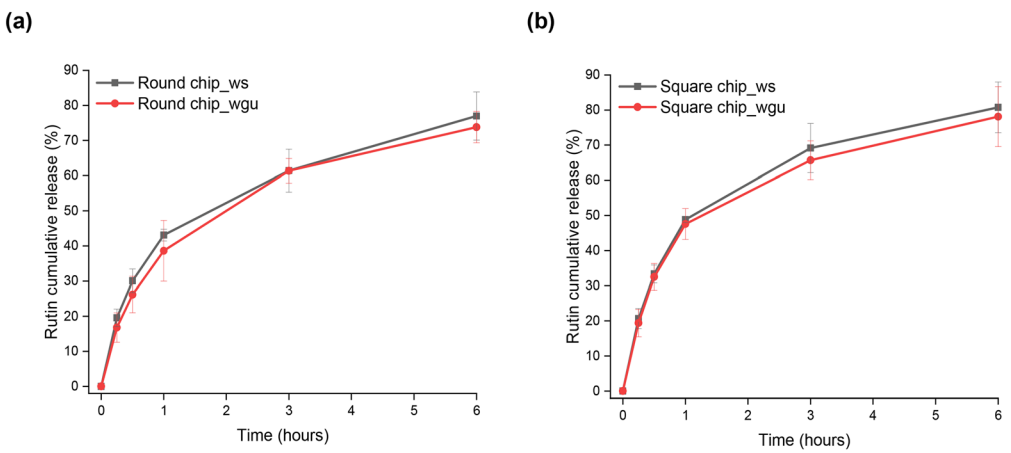

Fig. 6 Rutin release kinetics and corresponding mathematical models. Cumulative percentage of rutin mass released from round (a) and square (b) ZR-coated channels. All experiments with different simulated blood fluids (water/salts "ws" or water/glycerol/urea "wgu") were conducted at 37 °C. Data are presented as mean ± SD (n = 3), which were statistically analyzed using Student's t-test.

Table 2 Mathematical model fitting values obtained from rutin release kinetics. The table shows the comparison of correlation coefficients (r^2) obtained from fitting rutin release data through the proposed mathematical models. Bold numbers indicate the highest r^2 values for each type of experiment

Cross-section	SBF type	Zero order	First order	Higuchi	Korsmeyer–Peppas		Hixson–Crowell
		r^2	r^2	r^2	r^2	n	r^2
Round	ws	0.8996	0.9764	0.9745	**0.9774**	0.4198	0.9564
Round	wgu	0.8908	0.9618	0.9723	**0.9805**	0.4653	0.9414
Square	ws	0.8457	0.9517	0.9446	**0.9565**	0.4193	0.9215
Square	wgu	0.8462	**0.9492**	0.9434	**0.9489**	0.4226	0.9199

best fits with a higher correlation ($r^2 > 0.99$) were found to be Korsmeyer–Peppas' and Higuchi's equations (Table S3†). In particular, after fitting the first release data with the Korsmeyer–Peppas model, results showed high linearity with slope values between 0.5 and 1.0, indicating that the release rate is controlled by diffusion, relaxation (swelling), and erosion of the zein polymeric coatings as already pointed out by Fig. S3 and S4.†[52] By analyzing the second time period (60 minutes–6 hours), the highest r^2 values were observed for the Korsmeyer–Peppas and first-order models, with the latter referring to a system where the drug release rate is a function of the remaining drug concentration. Consistently, the n coefficients resulting from the Korsmeyer–Peppas model lie below 0.5 and confirm that the release kinetics were mainly diffusion-controlled over the last time period. The release kinetics of a hydrophilic drug, such as rutin, from a partially hydrophobic matrix, such as zein, generally involve both diffusion and matrix erosion. A similar explanation was reported by Berardi *et al.* regarding the drug release mechanism of tramadol from zein tablets in phosphate buffer solutions.[45] Overall, the mathematical modeling confirmed that the rutin release behavior is partially affected by the degradation process of the zein coatings: (1) the initial burst release is due to the rapid displacement of physically-adsorbed rutin molecules in the zein coatings; (2) pores are formed within the amphipathic zein matrix upon the release of the active ingredient and water contact; (3) the pores in the zein matrix constitute a transport pathway for the drug, allowing more water molecules to enter, thus facilitating rutin diffusion through the polymeric phase throughout the 6-hour experimental period.

Compared to the static experiments reported in our previous work,[21] both zein degradation and rutin release were found to be faster and more continuous when operating under dynamic conditions. The most likely explanation of these outcomes is that the constant liquid flow resulted in a more rapid infiltration of water within the polymer matrix and, as a consequence, in a constant removal of the drug/polymer top surface (*i.e.*, maintenance of the continuous concentration gradient and avoidance of the risk of medium saturation), such that the polymer degradation is accelerated.

3.5 Static blood cell adhesion and hemolysis assays

The occurrence of stent thrombosis has accelerated technological evolution in interventional cardiology, and the eradication of this fatal outcome should be the focus of new DESs.[53] Material hemocompatibility involves several key parameters, including wettability, chemical composition, surface charge, and roughness, which all affect cell and protein adsorption during the early response after a material–blood contact.[10,54] In this study, several samples were pre-conditioned as described in paragraph 2.10 and incubated in fresh mouse blood for 30 minutes under static conditions at 37 °C. As previously mentioned in paragraph 2.10.2, the altered morphology and protrusion of filopodia from adhered platelets can be taken as evidence of platelet activation. Fig. 7(a) and S4(a)† report the adhered and activated platelet levels on each prepared sample surface and control material. According to the data in Fig. 7(a), the average number of adherent and activated platelets per mm^2 was 617 (of which 333 showed activated morphology) and 775 (of which 179 showed activated morphology) on the zein-based coatings without and with rutin, respectively. For comparison reasons, a bare 316L SS surface was also tested, leading to average numbers of adherent and activated platelets per mm^2 of 2877 and 2489, respectively. The majority of the platelets on steel (Fig. 7(b)) showed aggregation, marked filopodia formation, and shape changes (spreading), as already reported in previous studies.[42] The same experimental protocol has also been followed for testing other reference materials (PU and PLA), currently under study in the literature as potential DES coatings. The average number of adherent and activated platelets per mm^2 were 2930 and 808 for the PU coating and 790 and 156 for the PLA coating, as shown in Fig. S5.† As a comparison with different naturally-derived materials, Kim *et al.* studied the platelet adhesion phenomena on alginate hydrogel films, with and without $CaCl_2$ crosslinking, which showed a density of 700 platelets per mm^2 and 840 platelets per mm^2, respectively.[55] A comparable number of cells was found on silk films, while several authors tested chitosan for its anti-thrombotic activity and measured more than 3500 adherent platelets per mm^2 on chitosan-coated surfaces.[56,57] On the other hand, the low amount of platelets adherent to our zein-based coatings might be ascribed to the partial hydrophobicity of the corn-derived material. Several authors claimed that surfaces containing the hydrophilic part of polar functional groups typically tend to favor cell attachment as compared to nonpolar hydrophobic surfaces.[10,46] Although many of the platelets adhering to the zein coating assumed a dendritic shape (Fig. 7(c)), very few platelets spread fully on

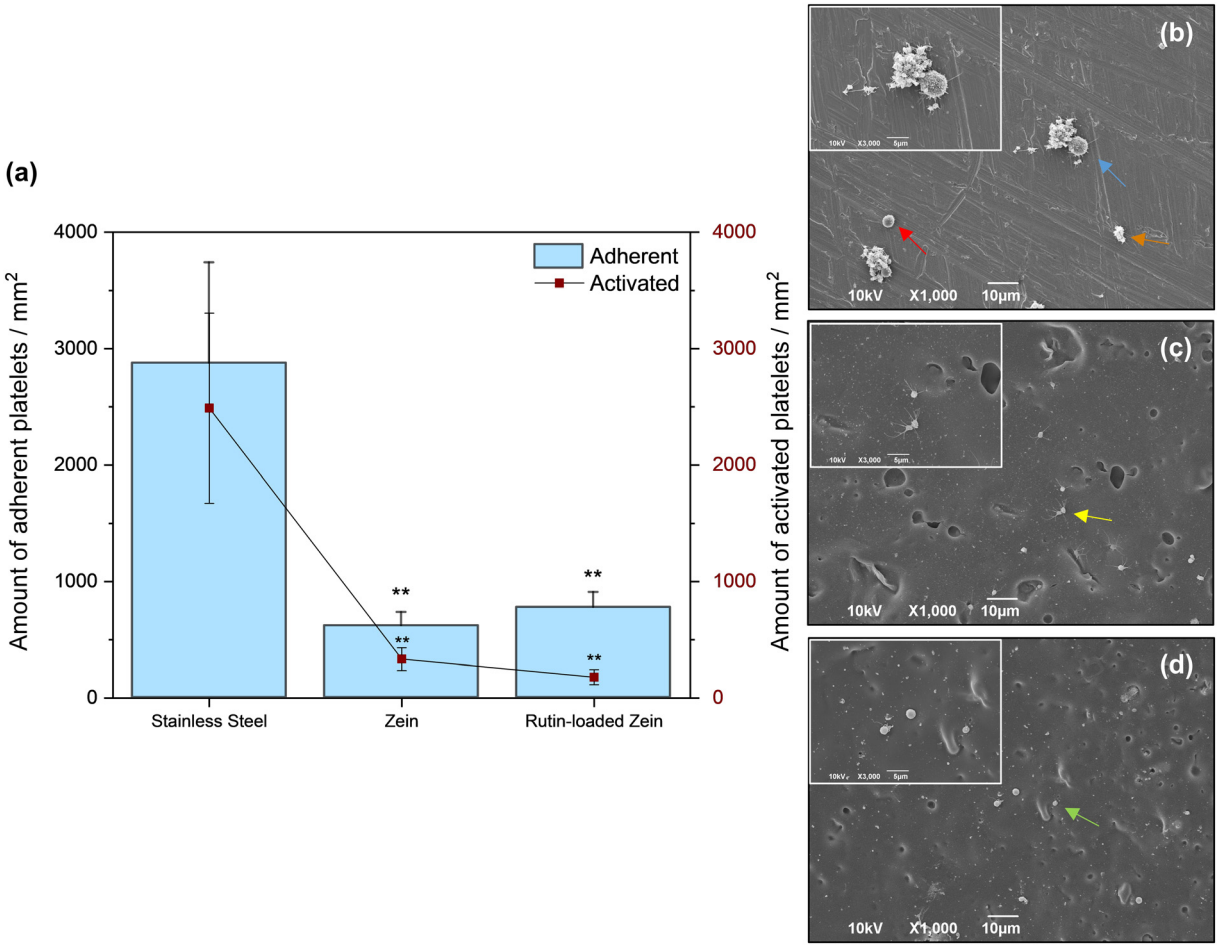

Fig. 7 Static hemocompatibility tests. The amount of adhered and activated platelets on different surfaces is shown in figure (a). Data are presented as mean ± SE, which were statistically analyzed using one-way ANOVA followed by *post hoc* Tukey's test, ** $p < 0.01$. Representative SEM images with magnified insets show the morphology of the platelets adhered on stainless steel (b), zein (c), and rutin-loaded zein (d). Arrows indicate red blood cells (red), white blood cells (cyan), resting platelets (green), activated platelets with filopodia (yellow), and aggregated platelets (orange).

the rutin-loaded coated surface, where a decrease in platelet activation was observed (Fig. 7(d)), and only a few platelets started to assume a dendritic (*i.e.*, partially activated) morphology. This result could be ascribed to (1) the electrostatic repulsion between the negative charges pertaining to the platelet and the rutin molecules and (2) the inherent anti-coagulant properties of the drug itself, which has been previously studied to effectively suppress platelet activation and thrombus formation.[58,59]

Erythrocyte-induced hemolysis *in vitro* is considered another reliable and important parameter to evaluate material hemocompatibility. Distilled water and saline solution were used as positive and negative controls. The hemolysis rates of zein-based films and reference samples after being incubated with whole blood at 37 °C for 30 minutes are summarized in Tables 3 and S4.† The zein and rutin-loaded zein samples revealed low hemolysis rates of 3.66 ± 1.02% and 2.43 ± 0.63%, respectively, which are lower than the judging criterion (5%) for eligible blood compatibility for any implantable biomedical materials, according to the ISO 10993-4 norm.[36] Other coatings fabricated from different naturally-derived materials (*e.g.*, silk fibroin, β-glucan, chitosan, and collagen) show similar hemolysis rates of less than 5%.[60–62] A low percentage of hemolysis was also observed for bare stainless steel (1.20 ± 0.54%) and PLA-coated samples (3.00 ± 0.21%), as confirmed by the data already available in the literature, while PU-coated samples showed a hemolysis rate of more than 20% and resulted in non-hemocompatible substrates.[42,63] Taken together, these data suggest that our zein-based coatings do not induce red blood cell hemolysis when they come into contact with blood, in accordance with the published literature.[44]

Table 3 Hemolysis rate for stainless steel and zein-based coatings

Sample surface	Hemolysis rate (%)
Normal saline (negative control)	0
Distilled water (positive control)	100
Stainless steel	1.20 ± 0.54
Zein	3.66 ± 1.02
Rutin-loaded zein	2.43 ± 0.63

3.6 Whole blood flow dynamic experiments

A preliminary analysis was performed to investigate the adhesion of PS beads and the consequent coating morphology after 30 minutes of flow of particulated SBFs. The attachment of the 5 μm diameter particles, mimicking the red blood cells' (RBCs) size, negative charge, density, and concentration in human blood could give an initial insight into the tendency of the coating to attract and allow adherence of flowing cells on itself. According to the SEM images (Fig. S6†), PS bead adhesion on the coated surface was very low, even though they were abundant in the fluids (5×10^6 beads per mL).

To investigate the blood compatibility of the ZR coating and the suitability of the microfluidic device for testing coating hemocompatibility, a dynamic whole blood test was performed at a flow rate of 500 μL min^{-1} for 10 minutes. Thrombus formation tends to occur within 5–8 minutes on most surfaces, despite the fact that several research groups have often set the flow time around 4–5 minutes using parallel-flow chambers.[20,64] Moreover, while numerous studies exclusively use platelet-rich plasma (PRP) when testing blood compatibility on selected materials, in our work the cumulative contributions of blood cells, coagulation factors, and hemodynamic forces were uniquely integrated into the process of thrombus formation by performing whole-blood flow tests. After the perfusion experiment, the formation of blood clots, platelet adhesion, and morphologies within the microfluidic channel were examined. Clot formation generally serves as one of the most important *in vitro* indicators for assessing the blood compatibility of a biomaterial. Under blood flow, the formation of clots is largely fueled by the adsorption of plasma proteins followed by the adhesion of blood cells on the implant surface.[10] In addition, the shape and size of platelets can change within a few seconds in response to an activating stimulus, with the activation level of adherent platelets being closely connected with their morphology. For example, platelets usually extrude filopodia upon activation, assuming a dendritic shape until completely spread.[54] Although only a limited number of papers have reported the usage of SEM images for evaluating both platelet adhesion and activation after performing dynamic blood assays, we decided to inspect our sample with electron microscopy techniques rather than fluorescence methods.[65–67] Nevertheless, being light-transparent, our chips could also be used in combination with brightfield and fluorescence microscopy. Representative SEM images acquired after the dynamic blood experiments are depicted in Fig. 8(a–c) which show a small number of platelets adhering onto the ZR coating (~3.2% area coverage) and only occasionally visible red blood cells. For comparison, Ollivier *et al.* reported a value of ~18% from the platelet coverage experiment on bare cobalt–chromium discs within 10 minutes of flow.[68] Under the same conditions, Sarvepalli *et al.* showed that platelet adhesion on a collagen-coated surface had exceeded 80% of the available surface area in a microfluidic chamber.[69] No presence of fibrin networks containing trapped blood cells, no clots or aggregation of platelets were found on the surface of our zein-based coatings. More interestingly, the imaged platelets present a round discoid shape (Fig. 8(b)) with a rare formation of filopodia sprouting from their surface, indicating a non-activated phenotype. In comparison to the images acquired after the experiments with SBF aqueous solutions (Fig. 5 and S2(a)†), SEM images of the zein matrix tested under blood flow (Fig. 8(a–c)) revealed more intense degradation, most likely due to the enzymatic action exerted on the polymer, as expected from the previous results obtained by Suarato *et al.*[70] Data obtained from the static tests are consistent with those from the dynamic whole blood tests and showed how this plant-derived drug-loaded matrix could provide a safe coating material for stent application. Our results are particularly relevant to the physiological situation in partially occluded blood vessels, where platelet behavior can significantly impact the onset of adverse effects and is of major interest when developing materials for stent coating.

4. Conclusions

This work reports the design and validation of simple, reusable, fused silica-based microfluidic platforms that enable the effect of the flow environment on the release kinetics of a degradable DES coating to be quantitatively analyzed. The developed microfluidic system could be employed to study different working fluids and flow rates and could accommodate several coating types (degrading or non-degrading) that can be deposited using various techniques (such as casting and spray

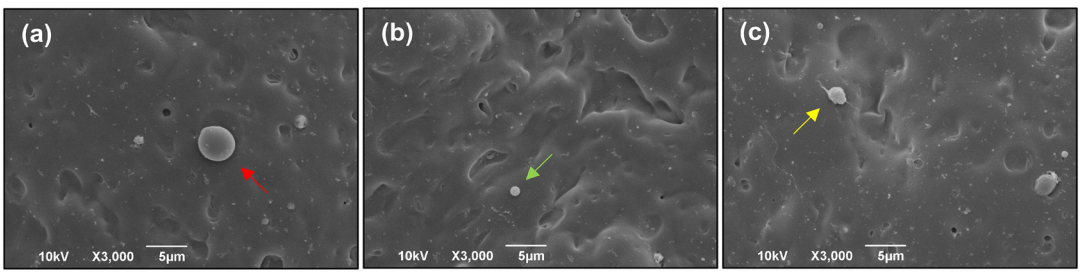

Fig. 8 Whole blood dynamic experiments on zein-based coated channels. SEM image of adherent blood cells on the ZR-coated microfluidic channel acquired after a 10 minutes flow. A red blood cell (red arrow), resting discoid platelet (green arrow), and slightly activated platelet with filopodia formation (yellow arrow) are shown in (a), (b), and (c), respectively.

methods). The current study focused on the effect of different SBFs and geometrical characteristics of the microfluidic channels on the degradation and drug release profiles of naturally-derived ZR coatings. Based on the assays we conducted, the release medium was found to affect the polymer degradation profile more than the geometrical shape of the channels. In particular, the zein matrix was degraded in a faster way when a higher concentration of salts was chosen and added to the eluting medium. The rutin delivery kinetics were then mathematically modeled to identify the drug release mechanism from the zein coatings, which was found to be diffusion-controlled (Fickian behavior), according to the Korsmeyer–Peppas model. The variations in polymer mass and surface topography of the films were also evaluated and compared to better understand the observed drug release behavior and could be used to guide future studies.

Hemocompatibility constitutes another leading requirement when designing blood-contacting materials for vascular device application. While the dynamics of blood cell activation are frequently overlooked during blood tests, which focus on local static cell-material effects, in this work a whole blood assay was carried out under controlled physiological flow conditions using our fused silica-based microfluidic devices to evaluate the anti-thrombotic properties of our material. The ZR coating was found to be hemocompatible from the results of the hemolysis assays (<5%) and the static and dynamic whole blood cell adhesion experiments. In particular, a significant decrease in platelet adhesion and activation was found on the rutin-loaded zein coatings in comparison to the reference substrates. As suggested in previous studies, and here confirmed by our data with whole blood experiments, rutin was demonstrated to reduce the degree of platelet activation, *i.e.*, the morphology of the adherent platelets was mainly discoid and round, suggesting a non-activated phenotype.[58,59] The obtained results add to the already known properties of rutin described in the literature, such as favorable endothelial cell proliferation, inhibition of vascular smooth muscle cell growth, and antioxidant and anti-inflammatory effects.[71–74] These are all essential features for innovative DES coatings to ensure the long-term safety of the medical implant in the human body. Therefore, rutin may give an alternative or extra approach to the anti-proliferative drugs present in several commercial drug-eluting stents by reducing the activation of the coagulation and inflammation cascades and by stimulating, rather than blocking, the healing process.

Altogether, our microfluidic systems represent versatile tools for release, degradation, and hemocompatibility studies, mimicking stent design and blood vessel environment. The herein presented results demonstrate that our proposed microfluidic strategy can positively contribute to the future screening and formulation of new coating materials for DESs upon exposure to different flow dynamic conditions. More importantly, we demonstrated that our plant-based sustainable materials may potentially be used as a safe alternative for the surface coating of blood-contacting biomedical implants.

Author contributions

Martina Lenzuni: conceptualization, investigation, visualization, formal analysis, validation, writing – original draft. Silvio Bonfadini: conceptualization, methodology, investigation, validation, visualization, writing – original draft. Luigino Criante: conceptualization, methodology, validation, visualization, supervision, writing – review & editing. Filippo Zorzi: investigation, validation, visualization. Maria Summa: resources, investigation, validation, writing – review & editing. Rosalia Bertorelli: validation, supervision, writing – review & editing. Giulia Suarato: conceptualization, investigation, validation, visualization project administration, writing – review & editing. Athanassia Athanassiou: conceptualization, project administration, supervision, writing – review & editing.

Conflicts of interest

There are no conflicts to declare.

Acknowledgements

The authors would like to thank Dr. Roberto Donno (Laboratory of Polymers and Biomaterials, Istituto Italiano di Tecnologia) for his help with the viscosity measurements and Doriana Debellis (Electron Microscopy Facility, Istituto Italiano di Tecnologia) for her assistance with the biological sample preparation.

References

1 P. Roopmani, S. Sethuraman, S. Satheesh and U. Maheswari Krishnan, *RSC Adv.*, 2016, **6**, 2835–2853.
2 A. V. Finn, F. D. Kolodgie, J. Harnek, L. J. Guerrero, E. Acampado, K. Tefera, K. Skorija, D. K. Weber, H. K. Gold and R. Virmani, *Circulation*, 2005, **112**, 270–278.
3 H. M. van Beusekom, F. Saia, J. D. Zindler, P. A. Lemos, S. L. Swager-Ten Hoor, M. A. van Leeuwen, P. J. de Feijter, P. W. Serruys and W. J. van der Giessen, *Eur. Heart J.*, 2007, **28**, 974–979.
4 J. Kotani, M. Awata, S. Nanto, M. Uematsu, F. Oshima, H. Minamiguchi, G. S. Mintz and S. Nagata, *J. Am. Coll. Cardiol.*, 2006, **47**, 2108–2111.
5 R. Virmani, G. Guagliumi, A. Farb, G. Musumeci, N. Grieco, T. Motta, L. Mihalcsik, M. Tespili, O. Valsecchi and F. D. Kolodgie, *Circulation*, 2004, **109**, 701–705.
6 Q. Zheng, Z. Chu, X. Li, H. Kang, X. Yang and Y. Fan, *Polymer*, 2017, **9**, 618–630.
7 U. Gbureck, E. Vorndran and J. E. Barralet, *Acta Biomater.*, 2008, **4**, 1480–1486.
8 C. M. McKittrick, S. Kennedy, K. G. Oldroyd, S. McGinty and C. McCormick, *Ann. Biomed. Eng.*, 2016, **44**, 477–487.
9 M. Kamberi, S. Nayak, K. Myo-Min, T. P. Carter, L. Hancock and D. Feder, *Eur. J. Pharm. Sci.*, 2009, **37**, 217–222.
10 Kenry, K. P. Loh and C. T. Lim, *Small*, 2015, **11**, 5105–5117.

11 G. Simitian, M. Virumbrales-Muñoz, C. Sánchez-de-Diego, D. J. Beebe and D. Kosoff, *Lab Chip*, 2022, **22**, 3618–3636.
12 Z. Li and E. Seker, *Lab Chip*, 2017, **17**, 3331–3337.
13 B. Amoyav, Y. Goldstein, E. Steinberg and O. Benny, *Pharmaceutics*, 2020, **13**, 13.
14 B. J. van Meer, H. de Vries, K. S. A. Firth, J. van Weerd, L. G. J. Tertoolen, H. B. J. Karperien, P. Jonkheijm, C. Denning, A. P. Ijzerman and C. L. Mummery, *Biochem. Biophys. Res. Commun.*, 2017, **482**, 323–328.
15 F. Storti, S. Bonfadini and L. Criante, *Sci. Rep.*, 2020, **10**, 12910.
16 F. Simoni, S. Bonfadini, P. Spegni, S. Lo Turco, D. E. Lucchetta and L. Criante, *Opt. Express*, 2016, **24**, 17416–17423.
17 S. Bonfadini, F. Ciciulla, L. Criante, A. Zaltron, F. Simoni, V. Reshetnyak and L. Lucchetti, *Sci. Rep.*, 2019, **9**, 1062.
18 F. He, Y. Liao, J. Lin, J. Song, L. Qiao, Y. Cheng and K. Sugioka, *Sensors*, 2014, **14**, 19402–19440.
19 D. Kim, S. Finkenstaedt-Quinn, K. R. Hurley, J. T. Buchman and C. L. Haynes, *Analyst*, 2014, **139**, 906–913.
20 I. Provenzale, S. L. N. Brouns, P. E. J. van der Meijden, F. Swieringa and J. W. M. Heemskerk, *Micromachines*, 2019, **10**, 787.
21 M. Lenzuni, G. Suarato, D. Miele, R. Carzino, M. Ruggeri, R. Bertorelli, G. Sandri and A. Athanassiou, *RSC Adv.*, 2021, **11**, 24345–24358.
22 J. F. Bentzon, F. Otsuka, R. Virmani and E. Falk, *Circ. Res.*, 2014, **114**, 1852–1866.
23 M. Kolossváry, J. Karády, B. Szilveszter, P. Kitslaar, U. Hoffmann, B. Merkely and P. Maurovich-Horvat, *Circ.: Cardiovasc. Imaging*, 2017, **10**, e006843.
24 G. Unal, S. Bucher, S. Carlier, G. Slabaugh, T. Fang and K. Tanaka, *IEEE Trans. Inf. Technol. Biomed.*, 2008, **12**, 335–347.
25 Z. Jia, C. Ma and H. Zhang, *Coatings*, 2021, **11**, 1427.
26 M. C. Brindise, M. M. Busse and P. P. Vlachos, *Exp. Fluids*, 2018, **59**, 173.
27 A. C. Tas, *Acta Biomater.*, 2014, **10**, 1771–1792.
28 T. Tamura, in *Comprehensive Biomedical Physics*, ed. A. Brahme, Elsevier, Oxford, 2014, pp. 91–105.
29 M. L. Bruschi, in *Strategies to Modify the Drug Release from Pharmaceutical Systems*, Woodhead Publishing, 2015, ch. 5, pp. 63–86.
30 D. Calzavara, D. Ferraro, L. Litti, G. Cappozzo, G. Mistura, M. Meneghetti and M. Pierno, *Adv. Condens. Matter Phys.*, 2018, **2018**, 2849175.
31 J. Berry, F. J. Peaudecerf, N. A. Masters, K. B. Neeves, R. E. Goldstein and M. T. Harper, *Lab Chip*, 2021, **21**, 4104–4117.
32 R. Reimers, S. Sutera and J. Joist, *Blood*, 1984, **64**, 1200–1206.
33 Z. Zhang, J. Borenstein, L. Guiney, R. Miller, S. Sukavaneshvar and C. Loose, *Lab Chip*, 2013, **13**, 1963–1968.
34 S. Braune, M. Grunze, A. Straub and F. Jung, *Biointerphases*, 2013, **8**, 33.
35 M. Weber, H. Steinle, S. Golombek, L. Hann, C. Schlensak, H. P. Wendel and M. Avci-Adali, *Front. Bioeng. Biotechnol.*, 2018, **6**, 99.
36 ISO, ISO 10993-4. Biological evaluation of medical devices, 2022.
37 Y. Tomohiko, T. Kanji, H. Satoshi and O. Akiyoshi, *Biomaterials*, 2003, **24**, 2889–2894.
38 X. Wang, N. Shi, Y. Chen, C. Li, X. Du, W. Jin, Y. Chen and P. R. Chang, *Biomed. Mater. Eng.*, 2012, **22**, 143–150.
39 J. Chung, D. Jeong, G.-h. Kim, S. Go, J. Song, E. Moon, Y. H. Huh and D. Kim, *Sci. Rep.*, 2021, **11**, 10511.
40 A. Dimasi, M. Rasponi, F. Consolo, A. Redaelli and M. Slepian, *J. Heart Lung Transplant.*, 2017, **36**, S11–S12.
41 M. H. Periayah, A. S. Halim and A. Z. Mat Saad, *Int. J. Hematol. Oncol. Stem Cell Res.*, 2017, **11**, 319–327.
42 J. Fu, Y. Su, Y.-X. Qin, Y. Zheng, Y. Wang and D. Zhu, *Biomaterials*, 2020, **230**, 119641.
43 F. J. Maksoud, M. F. Velázquez de la Paz, A. J. Hann, J. Thanarak, G. C. Reilly, F. Claeyssens, N. H. Green and Y. S. Zhang, *J. Mater. Chem. B*, 2022, **10**, 8111–8165.
44 X. Liu, Y. Xie, W. Li, W. Sheng, Y. Li, Z. Tong, H. Ni, C. Huselstein, X. Wang and Y. Chen, *Biomed. Mater. Eng.*, 2015, **25**, 47–55.
45 A. Berardi, L. Bisharat, G. Bonacucina, L. Casettari, S. Logrippo, M. Cespi, H. S. AlKhatib and G. F. Palmieri, *Powder Technol.*, 2017, **310**, 241–249.
46 H. J. Wang, Z. X. Lin, X. M. Liu, S. Y. Sheng and J. Y. Wang, *J. Controlled Release*, 2005, **105**, 120–131.
47 T. Swaine, Y. Tang, P. Garcia, J. John, L. J. Waters and A. L. Lewis, *Eur. J. Pharm. Sci.*, 2016, **93**, 351–359.
48 A. I. Visan, G. Popescu-Pelin and G. Socol, *Polymer*, 2021, **13**, 1272.
49 O. Nødland, A. Lohne, A. Stavland and A. Hiorth, *Transp. Porous Media*, 2019, **128**, 1–27.
50 K. Hermans, D. Van den Plas, S. Kerimova, R. Carleer, P. Adriaensens, W. Weyenberg and A. Ludwig, *Int. J. Pharm.*, 2014, **472**, 10–19.
51 E. S. Bacaita, B. C. Ciobanu, M. Popa, M. Agop and J. Desbrieres, *Phys. Chem. Chem. Phys.*, 2014, **16**, 25896–25905.
52 P. Costa and J. M. Sousa Lobo, *Eur. J. Pharm. Sci.*, 2001, **13**, 123–133.
53 D. H. Lee and J. M. de la Torre Hernandez, *Eur. Cardiol.*, 2018, **13**, 54–59.
54 S. L. Goodman, T. G. Grasel, S. L. Cooper and R. M. Albrecht, *J. Biomed. Mater. Res.*, 1989, **23**, 105–123.
55 J. H. Kim, N. R. Ko, B.-Y. Jung and I. K. Kwon, *Macromol. Res.*, 2016, **24**, 931–939.
56 T. C. Chou, E. Fu, C. J. Wu and J. H. Yeh, *Biochem. Biophys. Res. Commun.*, 2003, **302**, 480–483.
57 M. Lovett, G. Eng, J. A. Kluge, C. Cannizzaro, G. Vunjak-Novakovic and D. L. Kaplan, *Organogenesis*, 2010, **6**, 217–224.
58 S.-S. Choi, H.-R. Park and K.-A. Lee, *Antioxidants*, 2021, **10**, 1696.
59 C. H. Lescano, F. Freitas de Lima, C. A. L. Cardoso, S. C. H. Vieira, F. Z. Mónica and I. Pires de Oliveira, *Food Funct.*, 2021, **12**, 802–814.
60 W. Xu, K. Yagoshi, T. Asakura, M. Sasaki and T. Niidome, *ACS Appl. Bio Mater.*, 2019, **3**, 531–538.

61 M. Michalska-Sionkowska, O. Warżyńska, B. Kaczmarek-Szczepańska, K. Łukowicz, A. M. Osyczka and M. Walczak, *Materials*, 2021, **14**, 1322.
62 Z. Wu, W. Zhou, W. Deng, C. Xu, Y. Cai and X. Wang, *ACS Appl. Mater. Interfaces*, 2020, **12**, 20307–20320.
63 J. Li, Q. Chen, Q. Zhang, T. Fan, L. Gong, W. Ye, Z. Fan and L. Cao, *ACS Appl. Mater. Interfaces*, 2020, **12**, 14365–14375.
64 R. Van Kruchten, J. M. Cosemans and J. W. Heemskerk, *Platelets*, 2012, **23**, 229–242.
65 L. H. Ting, S. Feghhi, N. Taparia, A. O. Smith, A. Karchin, E. Lim, A. S. John, X. Wang, T. Rue, N. J. White and N. J. Sniadecki, *Nat. Commun.*, 2019, **10**, 1204.
66 A. Jain, A. Graveline, A. Waterhouse, A. Vernet, R. Flaumenhaft and D. E. Ingber, *Nat. Commun.*, 2016, **7**, 10176.
67 C. Minelli, A. Kikuta, N. Tsud, M. D. Ball and A. Yamamoto, *J. Nanobiotechnol.*, 2008, **6**, 3.
68 V. Ollivier, C. Roques, N. Receveur, M. Gratz, L. Feldman, D. Letourneur, C. Gachet, P. H. Mangin and M. Jandrot-Perrus, *Platelets*, 2017, **28**, 529–539.
69 D. P. Sarvepalli, D. W. Schmidtke and M. U. Nollert, *Ann. Biomed. Eng.*, 2009, **37**, 1331–1341.
70 G. Suarato, M. Contardi, G. Perotto, J. A. Heredia-Guerrero, F. Fiorentini, L. Ceseracciu, C. Pignatelli, D. Debellis, R. Bertorelli and A. Athanassiou, *Mater. Sci. Eng., C*, 2020, **116**, 111151.
71 T. M. Bedair, H. M. Bedair, K. W. Ko, W. Park, Y. K. Joung and D. K. Han, *Colloids Surf., B*, 2019, **181**, 174–184.
72 S. H. Yu, J. M. Yu, H. J. Yoo, S. J. Lee, D. H. Kang, Y. J. Cho and D. M. Kim, *Yonsei Med. J.*, 2016, **57**, 373–381.
73 W. Lee, S. K. Ku and J. S. Bae, *Food Chem. Toxicol.*, 2012, **50**, 3048–3055.
74 Z. Gao, H. Xu, X. Chen and H. Chen, *Life Sci.*, 2003, **73**, 1599–1607.